Materials Today 90 (2025) 132–142

Contents lists available at ScienceDirect

Materials Today

journal homepage: www.elsevier.com/locate/mattod

Exceptional flame-retardant, super strong/tough, and superhydrophobic/self-cleaning wood

Feng Gu [a], Xianhao He [a], Youhang Wei [a], Xiuxue Niu [a], Zhaosheng Cai [a], Bo Jiang [b], J.Y. Zhu [c,*], Wangxia Wang [a,*]

[a] School of Chemistry and Chemical Engineering, Yancheng Institute of Technology, Yancheng 224051, China
[b] Jiangsu Co-Innovation Center of Efficient Processing and Utilization of Forest Resources, Nanjing Forestry University, Nanjing 210037, China
[c] USDA Forest Service, Forest Products Laboratory, Madison, WI 53726, USA

ARTICLE INFO

Keywords:
Wood
Flame retardant
Superhydrophobic
Densification
Dip-coating

ABSTRACT

This study presents a novel approach to fabricate wood composites with exceptional flame retardancy, superior strength and toughness, as well as superhydrophobic/self-cleaning properties. The fabrication process involves densifying delignified wood pre-impregnated with a nitrogen-phosphorus flame retardant via hot-pressing, followed by an adhesive-free, self-curing superhydrophobic dip-coating. The resulting wood exhibits remarkable synergistic performance: exceptional flame retardancy, with peak heat release rate (pHRR) and total heat release (THR) decreased by 77.7 % and 63.6 %, respectively, compared with pristine wood; superhydrophobicity/self-cleaning with a water contact angle (WCA) of 161.2° and sliding rolling off angle (SA) of 3.9°; and outstanding mechanical performance with a tensile strength of 439 MPa and fracture toughness of 8.7 MJ/m^3. Notably, this innovation addresses two critical challenges in fire-retardant wood technology—preventing flame retardant leaching and eliminating flammable adhesives—thereby offering a scalable method for the commercial production of high-performance wood composites suitable for applications in green architecture, transportation, and safety–critical infrastructure.

Introduction

Sustainable economic development mandates to find sustainable alternatives to energy and carbon intensive materials in buildings and constructions [1]. Wood is one of the most abundant plant-based renewable materials on Earth and has been used for construction historically [2]. Nonetheless, wood is highly flammable. The wildfires in Los Angeles, California, USA, in January 2025 destroyed more than 16,000 structures, citing the flammability of wooden homes and furniture as the main cause [3].

Incorporating flame retardants into wood can be an effective approach to enhance wood fire resistance [4]. However, impregnating halogenated flame retardants into wood cannot meet the health requirements for modern buildings due to the risk of bioaccumulation in human bodies [5]. In recent decades, intumescent flame retardants, composed of acid, gas, and char-forming agents, have gained considerable attention due to their high efficacy, low smoke emission, and low toxicity [6–8]. Ammonium polyphosphate (APP), a nitrogen-phosphorus intumescent compound, decomposes upon heating to form a dense phosphorus-rich char layer on wood surface that can physically insulate heat and oxygen to prevent direct flame-wood contact [9]. Polyethyleneimine (PEI), a hyperbranched nitrogen-rich cationic polyelectrolyte, significantly enhances flame retardancy by not only scavenging free radicals such as H^+ and OH^- from wood combustion to interrupt combustion chain reactions, but also forming covalent bonds with APP via cation exchange reactions. This chemical interaction stabilizes APP within the matrix, improves its dispersion, and creates a synergistic P-N-C network that promotes the formation of a more thermally stable char layer [10]. However, the inherent hygroscopicity of wood inevitably can leach water-soluble flame retardants such as PEI in practical applications, thereby compromising the long-term durability of flame-retardant performance [11,12].

Inspired by the liquid-repellent surfaces of various natural materials, we hypothesize that superhydrophobic coatings with self-cleaning properties can mitigate the loss of flame retardants from hygroscopic wood through leaching by hindering water permeation [13]. To

* Corresponding authors.
E-mail addresses: junyong.zhu@usda.gov (J.Y. Zhu), wang.w.xia@ycit.edu.cn (W. Wang).

https://doi.org/10.1016/j.mattod.2025.08.034
Received 30 July 2025; Received in revised form 23 August 2025; Accepted 31 August 2025
Available online 3 September 2025
1369-7021/Published by Elsevier Ltd.

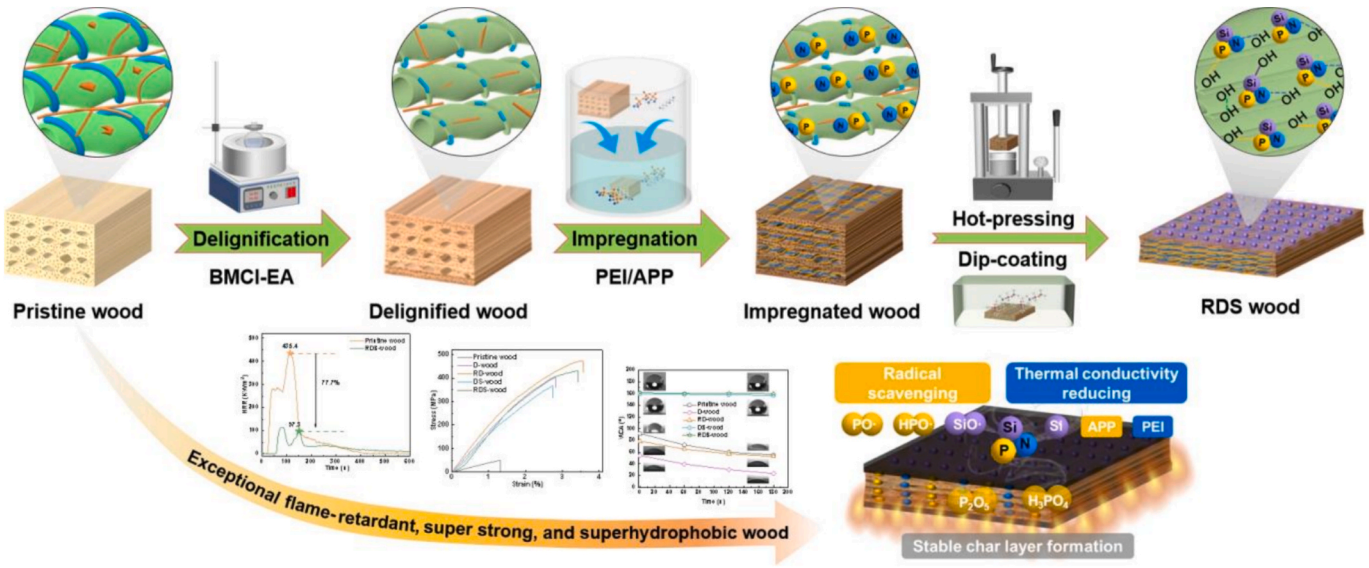

Fig. 1. A schematic flow diagram shows the processes employed for producing an exception flame-retardant, super strong/tough, and superhydrophobic/self-cleaning wood.

fabricate super liquid-repellent layers, two essential features are generally required: a micro- or nanostructured surface texture and a nonpolar surface chemistry [14]. Nano-silica is commonly employed to fabricate hierarchical nanostructures on wood substrates, working in tandem with low-surface-energy polydimethylsiloxane (PDMS) to create a superhydrophobic surface [15,16]. Notwithstanding, the incorporation of epoxy resin and curing agents is often necessary to improve coating durability [17]. However, the flammable nature of epoxy resin can compromise the flame-retardant performance of the resultant wood. It is known that tetraethyl orthosilicate (TEOS) has self-curing properties and can form gel with the backbone of PDMS in-situ via hydrolysis and condensation under ammonia catalysis [18]. The process was demonstrated on textile cellulose fibers [19] but not on wood that contains lignin. Here we propose an innovative approach: utilize the self-curing and gelation properties of TEOS with PDMS to generate an interpenetrating superhydrophobic nano-silica network structure on wood surface without either epoxy resins or curing agents, in stark contrast to using adhesives to fix superhydrophobic silica coating on wood surface. Our approach eliminates the use of flammable organic components and addresses the flame retardancy durability and issues associated with traditional flammable epoxy-based systems.

With this approach as schematically shown in Fig. 1, our study is to demonstrate immobilizing flame retardants on wood through mechanical hot-pressing to densify delignified wood pre-impregnated with flame retardants followed by chemical adhesive-free self-curing superhydrophobic dip-coating of PDMS/TEOS. This addressed two critical challenges: flame retardancy degradation caused by flammable adhesives in conventional superhydrophobic coatings and hygroscopicity-induced flame-retardant leaching. Delignified wood was first impregnated with PEI/APP and then hot-pressed to physically and chemically immobilize flame retardants. The resultant densified wood was dip-coated with PDMS/TEOS to form an adhesive-free self-curing superhydrophobic layers through ammonia-catalyzed sol–gel reactions to generate a superhydrophobic PDMS-silica coating layer. This dual strategy resulted in a multifunctional wood with exceptional flame retardancy, outstanding mechanical strength, and durable superhydrophobic surface even after mechanical abrasion, and acidic or alkaline chemical corrosion.

The novelties of the present study are: (1) Proposing a dual-strategy (mechanical hot-pressing for flame retardant immobilization and adhesive-free self-curing superhydrophobic dip-coating) that has not been reported in PEI/APP-related wood flame-retardant research to simultaneously address flame retardant leaching and flammable adhesives in conventional coatings. (2) Utilizing TEOS self-curing property under ammonia catalysis to construct an interpenetrating network with PDMS for improving coating stability and enhancing both superhydrophobic durability and flame retardancy, very different from traditional PEI/APP applications using flammable adhesives such as epoxy resin. (3) Systematically demonstrating that combining hot-pressing and self-curing dip-coating can significantly mitigate flame retardant loss in high-humidity environments, providing a novel solution for long-term durable fire safety of wood structures in high-humidity environments, in contrast to existing methods focusing only on short-term flame-retardant effects using PEI/APP. (4) Densifying wood through hot-pressing which also resulted in a wood of outstanding mechanical performance in addition to exceptional flame retardant, never reported in existing fire retardant wood literature but needed as flame retardant wood often has a low mechanical strength [12].

Results and discussion

Wood chemical characteristics and mechanical strength

Wood samples are labelled using the abbreviations of the processes applied to facilitate discussion, i.e., impregnation with flame retardant PEI/APP as *R*, densification through hot-pressing as *D*, dip-coating with the adhesive-free superhydrophobic solution as *S*. Therefore, the R-wood refers to delignified wood impregnated with flame-retardants without densification. The D-wood is simply the densified delignified wood without flame-retardant impregnation and superhydrophobic dip-coating. RDS-wood stands for flame retardant impregnated and densified superhydrophobic wood. RD-wood and DS-wood stand for densified wood samples without dip-coating with superhydrophobic coating, and superhydrophobic wood without flame retardant impregnation, respectively.

FTIR and XPS were employed to characterize the surface chemical structure of wood. For RD-wood, the infrared band at 1650 cm^{-1} corresponds to the amide I band (C═O stretching vibration of —CONH— groups), while the band at 1100 cm^{-1} is assigned to the C—N stretching vibration in amide linkages. The peaks at 1258 cm^{-1} and 1020 cm^{-1} are stretching vibration of P═O and P—O—C, respectively (Fig. 2a) [20]. For DS-wood, the infrared band at 1080 cm^{-1} is attributed to the stretching vibration of Si—O, and the band at 800 cm^{-1} is due to the stretching vibration of Si—C [21] (Fig. 2a). All these bands of RD-wood

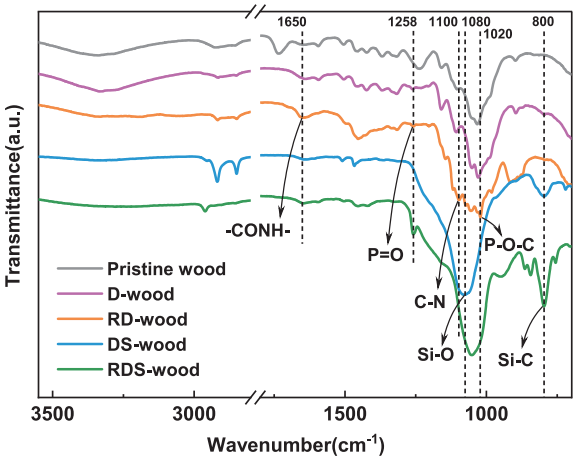

(a) FTIR spectra of wood

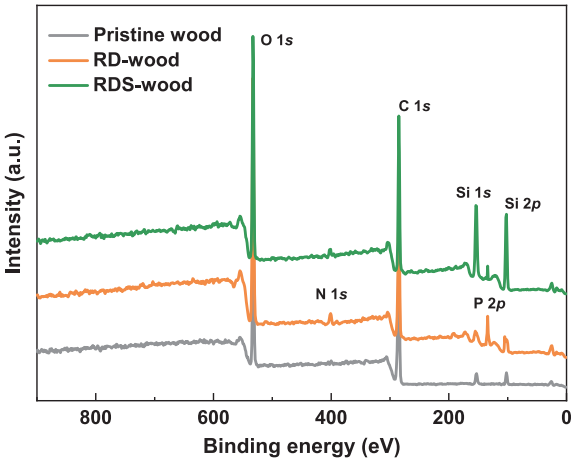

(b) XPS survey spectrum of wood

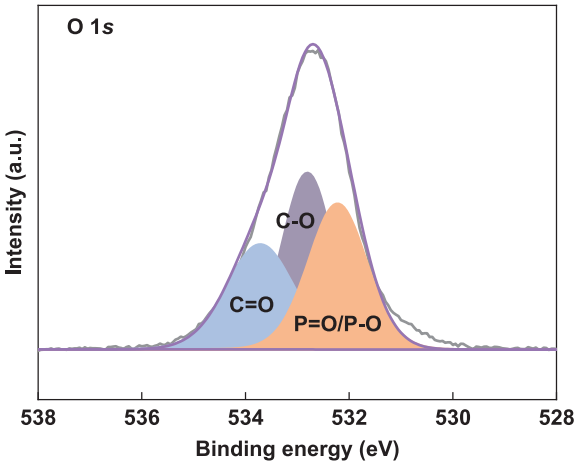

(b1) O 1*s* XPS spectra of the RDS-wood

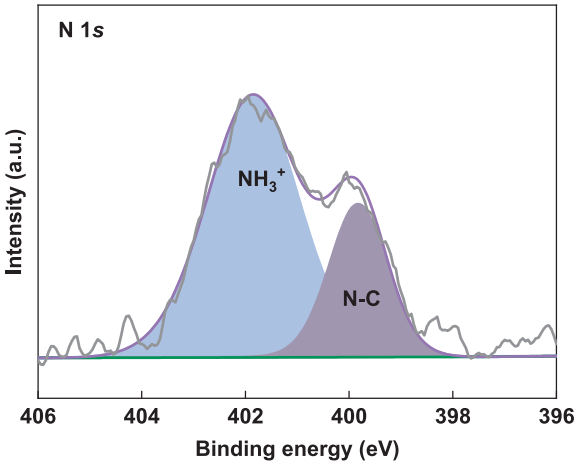

(b2) N 1*s* XPS spectra of the RDS-wood

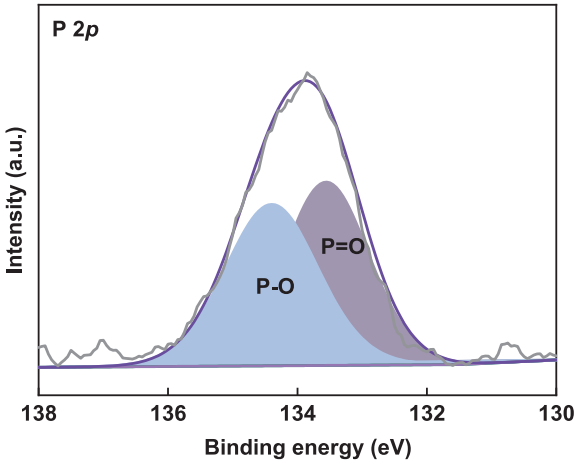

(b3) P 2*p* XPS spectra of the RDS-wood

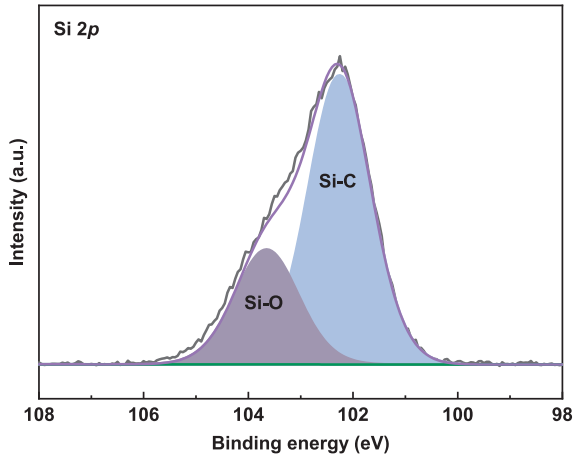

(b4) Si 2*p* XPS spectra of the RDS-wood

Fig. 2. FTIR and XPS spectra of wood samples (a) FTIR spectrum. (b) XPS spectrum.

and DS-wood were also detected in RDS-wood as shown, suggesting both flame-retardant and superhydrophobic modifications were successfully implemented on RDS-wood.

Results from XPS analysis can reveal the surface chemical characteristic of the wood samples produced in this study. As shown in Fig. 2b. Peaks observed at 533, 401, 287, 134, and 103 eV were attributed to O1*s*, N1*s*, C1*s*, Si2*p*, and P2*p* orbitals, respectively [22]. In the O1s spectrum (Fig. 2b1), three peaks at 533.7 eV (C═O), 532.8 eV (C—O), and 532.2 eV (P—O or P═O) were identified. The N1*s* spectrum (Fig. 2b2) exhibited peaks at 401.8 eV and 399.8 eV, corresponding to NH_3^+ and N—C groups, respectively. In the P2*p* spectrum (Fig. 2b3), peaks at 134.4 eV and 133.6 eV were assigned to P═O and P—O bonds.

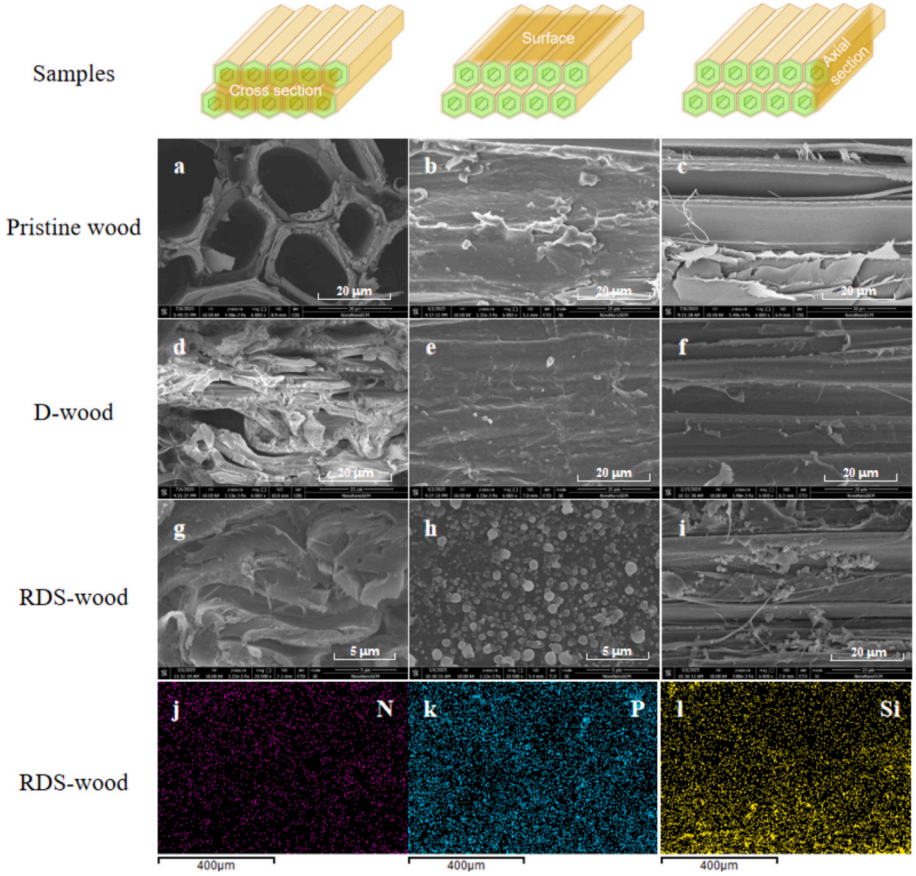

Fig. 3. SEM images of wood samples (a–c) Pristine wood. (d–f) D-wood. (g–i) RDS-wood. (j–l) EDS mapping of RDS-wood.

Finally, the Si2*p* spectrum (Fig. 2b4) displayed peaks at 103.6 eV (Si—O) and 102.2 eV (Si—C), confirming the presence of a crosslinked siloxane network on the wood surface.

Both FTIR and XPS spectra confirmed the effective incorporation of flame-retardant and hydrophobic components into RDS-wood. SEM imaging (Fig. 3) further revealed the successful formation of a superhydrophobic nanolayer on the RDS-wood surface (Fig. 3h). Furthermore, energy dispersive X-ray spectroscopy (EDS) mapping demonstrated the uniform distribution of PEI, APP, and SiO_2 within the wood substrate (Fig. 3j–l). FTIR analysis indicated potential hydrogen-bonded crosslinking networks between amino groups in PEI/APP and hydroxyl groups in cellulose, hemicelluloses, and residual lignin, as suggested by the weakened–OH peak in the spectra of the modified wood compared with pristine wood. Meanwhile, the characteristic peaks corresponding to –CONH– and P–O–C groups indicate the formation of covalent linkages, attributed to hot-pressing-induced polycondensation reactions between the flame retardants and wood polymeric components, which are important to immobilize flame retardant. These synergistic interactions not only enhanced wood rigidity by restricting the viscoelastic deformation of polymeric chains with RD-wood tensile strength of 480 ± 8 MPa, but also mitigated flame-retardant leaching by chemically anchoring APP and PEI within the wood's three-dimensional microstructure (Fig. 3g and i). However, the subsequent superhydrophobic modification might have disrupted pre-formed hydrogen bonds and weakened intermolecular forces to result in a slightly decrease in the mechanical strength of RDS-wood to 439 ± 9 MPa. Despite this decrease, RDS-wood exhibited a strain of 3.5 % and a toughness of 8.7 MJ/m^3, 26 times that of the pristine wood (Fig. 4a).

Superhydrophobicity of RDS-wood

Rough surface structures can amplify the intrinsic hydrophobicity of a material according to the Wenzel model [23] and the Cassie-Baxter model [24]. The hierarchical structures generated via TEOS hydrolysis acted synergistically with the low-surface-energy PDMS layer. This in-situ formation of an interpenetrating network (IPN) between TEOS-derived silica and PDMS significantly enhanced the superhydrophobicity of the resultant wood surface. This synergistic effect was evidenced by a remarkable increase in the water contact angle as shown in Fig. 4b, where nearly spherical droplets were observed on both DS-wood and RDS-wood surfaces. Notably, the initial water contact angle (IWCA) of the pristine wood was 91.7°. After delignification, the IWCA of the densified D-wood decreased to 54.4°, primarily due to the removal of relatively hydrophobic lignin and the increase in the smoothness of the wood surface. With PEI/APP impregnation, the IWCA of RD-wood increased to 78.9° as a result of tighter wood cell wall structures and decreased micropores/defects on the surface. Following the construction of a rough, low-surface-energy layer, the IWCA reached 159.5° on DS-wood and further increased to 161.2° on RDS-wood. The infiltration of flame-retardant agents repaired both internal and external surface defects of the wood, contributing to the enhanced surface hydrophobicity. This result outperforms silsesquioxane-grafted lignin-coated wood (WCA: 158°) [25] and PDMS/M−SiO_2−sprayed wood (WCA: 154°) [15].

The sliding rolling off angle of RDS-wood was extremely low (3.9°), enabling water droplets to roll over easily, which can carry away surface pollutants such as dust to exhibit self-cleaning behavior (Fig. 4d vs c). Moreover, the nanoscale superhydrophobic layers were quite stable under mechanical abrasion and chemical corrosion. Even after 80 cycles of sandpaper abrasion and immersing in acid, alkali, and salt solutions

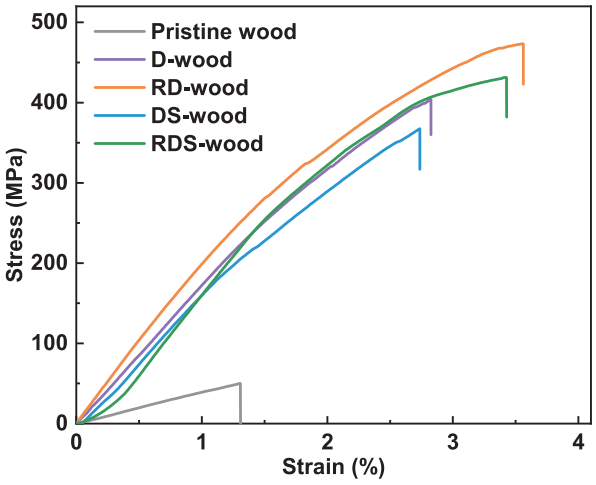

(a) Stress-strain curves of wood

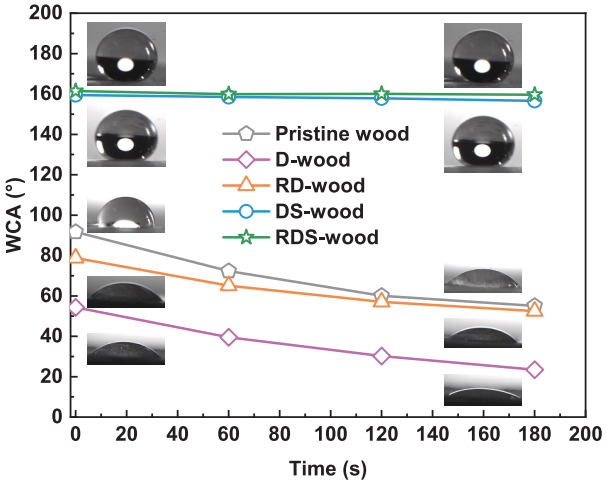

(b) Water contact angle of wood

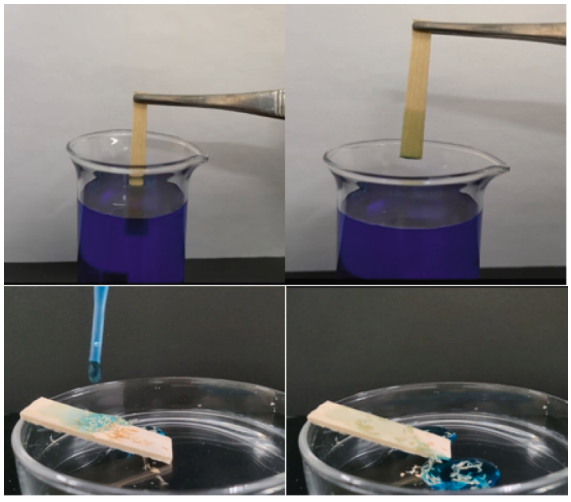

(c) Self-cleaning behavior of the pristine wood

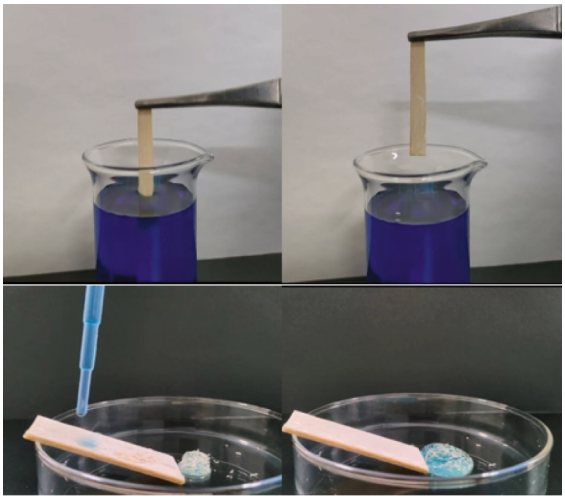

(d) Self-cleaning behavior of the RDS-wood

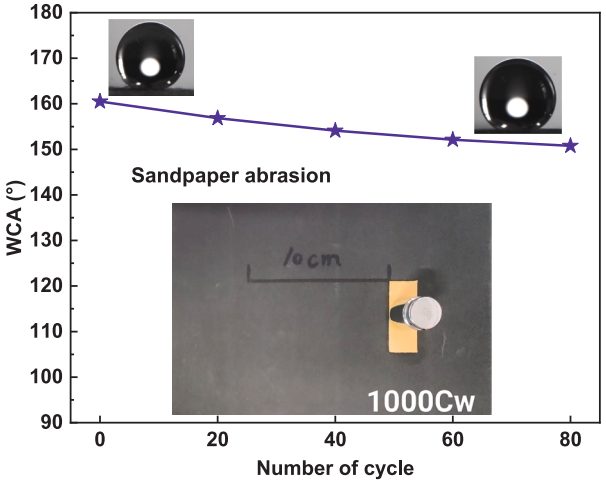

(e) Mechanical stability of the RDS-wood

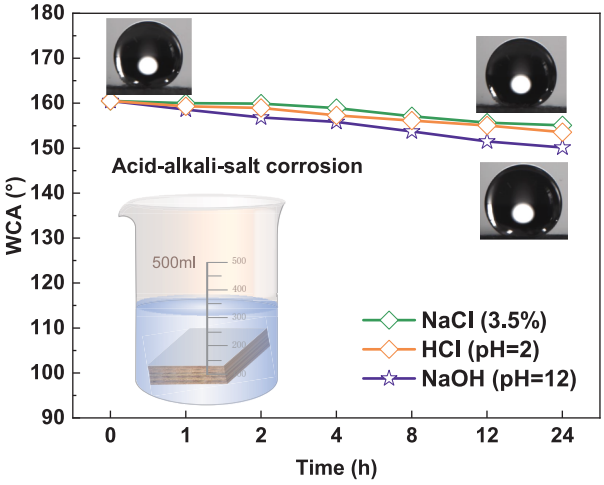

(f) Chemical stability of the RDS-wood

Fig. 4. Mechanical, surface, and stability properties of wood samples. (a) Stress–strain curves. (b) Water contact angles. (c) Self-cleaning behavior of the pristine wood. (d) Self-cleaning behavior of the RDS-wood. (e) Mechanical stability of the RDS-wood. (f) Chemical stability of the RDS-wood.

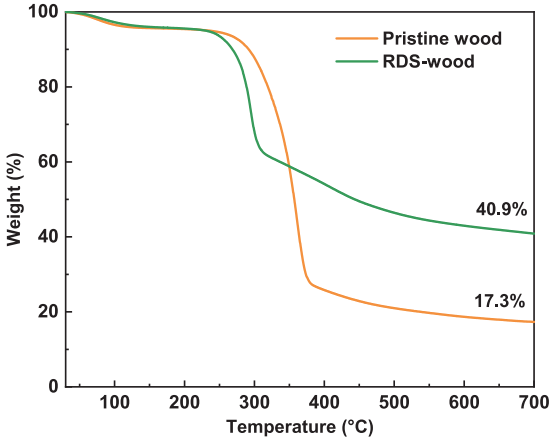

(a) TG curves of the pristine wood and the RDS-wood

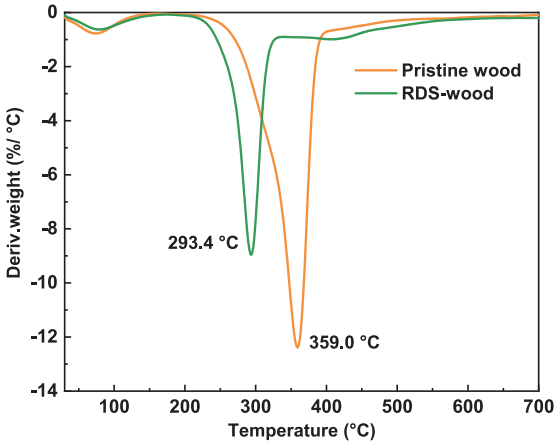

(b) DTG curves of the pristine wood and the RDS-wood

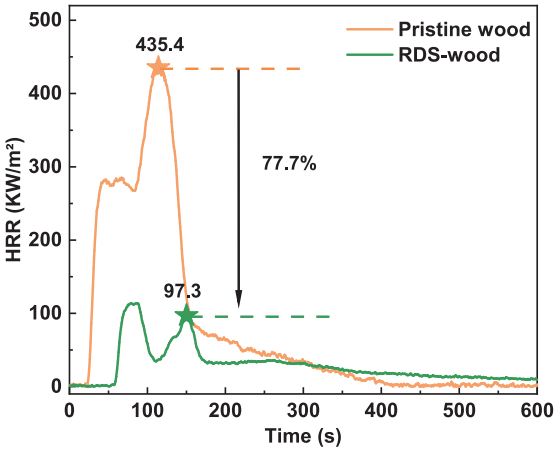

(c) HRR curves of the pristine wood and the RDS-wood

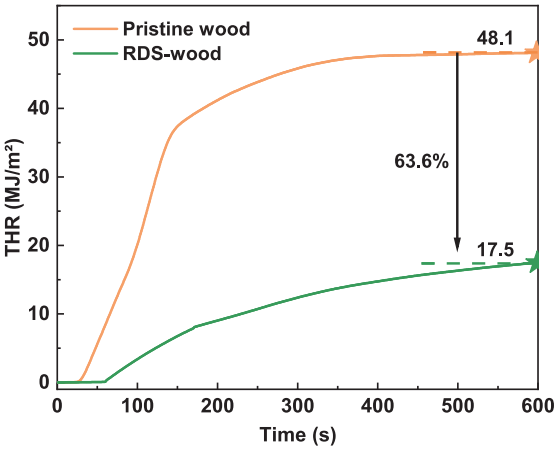

(d) THR curves of the pristine wood and the RDS-wood

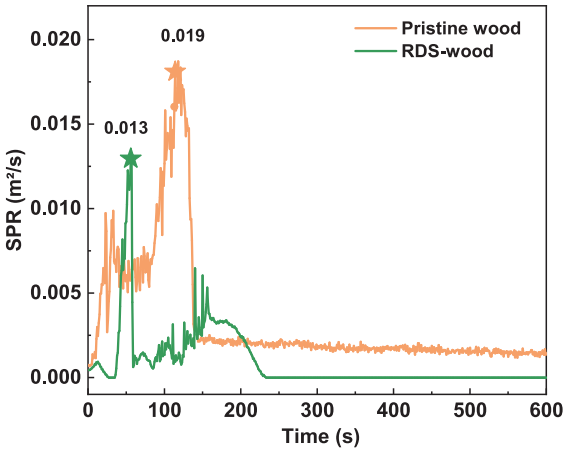

(e) SPR curves of the pristine wood and the RDS-wood

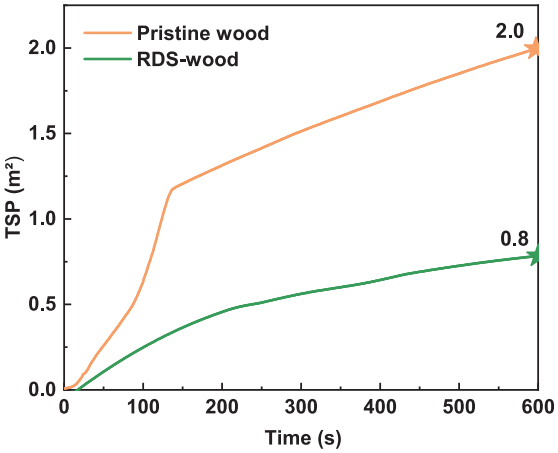

(f) TSP curves of the pristine wood and the RDS-wood

Fig. 5. Thermal and combustion performance curves of the pristine wood and the RDS-wood. (a) TG curves. (b) DTG curves. (c) Heat release rate (HRR) curves. (d) Total heat release (THR) curves. (e) Smoke production rate (SPR) curves. (f) Total smoke production (TSP) curves.

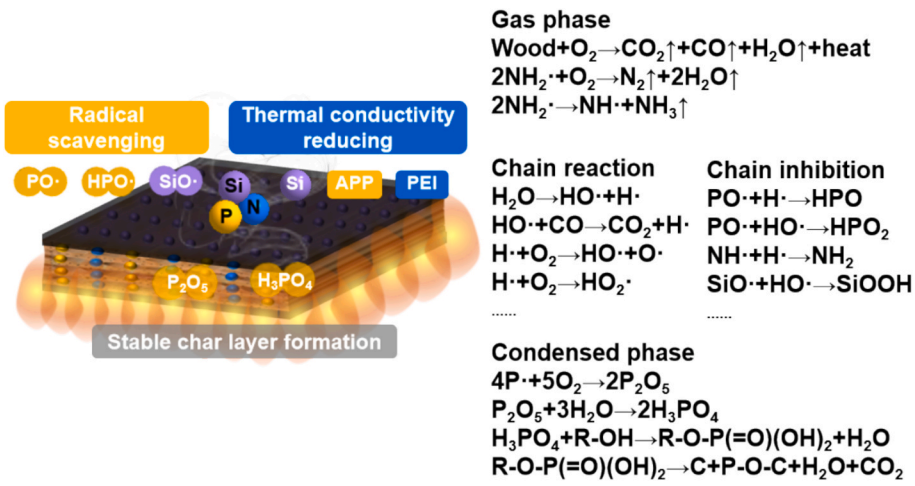

Fig. 6. Schematic illustration of the flame-retardant mechanisms of the RDS-wood.

for 24 h, the superhydrophobicity of the surface remained outstanding (Fig. 4e and f). This stable nano-rough layer with low surface energy can prevent the migration and leaching of impregnated flame retardants in high-humidity or wet environments [26].

Exceptional flame retardancy of RDS-wood

Thermal stability is a critical indicator of wood fire resistance [27]. As shown in Fig. 5a & b, RDS-wood exhibited lower initial and maximum degradation temperatures compared with the pristine wood, partly because the P-containing groups in the RDS-wood introduced by PEI/APP infiltration degraded at relatively low temperatures. The released acidic substances catalyzed the aggregation of small woody fragments to form a compact flame-retardant carbonaceous layer that inhibited further degradation at elevated temperatures [28]. The greater yield in carbon residue of 40.9 % from RDS-wood also acted as an efficient barrier to heat transfer and oxygen diffusion to inhibit combustion, thereby enhanced flame retardancy.

Cone calorimeter test data (Fig. 5c–d) revealed that the peak heat release rate (pHRR) of RDS-wood decreased from 435.4 kW/m^2 to 97.3 kW/m^2, and the total heat release (THR) decreased by 63.6 %, from 48.1 MJ/m^2 to 17.5 MJ/m^2. These significant decreases can be attributed to three synergistic mechanisms as shown in Fig. 6. First, the degradation of P-containing groups at low temperatures released acidic substances that promoted dehydration and cyclization of wood components and catalyzed the formation of a compact, thermally stable char layer (Table S2). This char layer, further reinforced by the silica network, physically blocked heat transfer to the underlying wood and restricted the diffusion of volatile combustible gases from pyrolysis (Fig. S1). The peak smoke production rate (pSPR) and total smoke production (TSP) were decreased from 0.019 m^2/s to 0.013 m^2/s, and 2.0 m^2 to 0.8 m^2, respectively, due to the decreasing availability of fuel for smoke formation (Fig. 5e–f). Second, the decomposition products from PEI and APP in RDS-wood scavenged free radicals from wood combustion to inhibit gas-phase combustion and further decreased pHRR and THR. This radical-scavenging mechanism was critical to interrupting the combustion cycle. In addition, the physical infiltration of PEI, APP, and silica into the wood matrix decreased wood thermal conductivity [18]. Specifically, the in-situ network formation between TEOS-derived silica and PDMS constructed a hierarchically structured matrix, which disrupted continuous thermal conduction paths. This slowed heat transfer within the wood, thereby delaying the heating and decomposition of internal woody materials and lowering pHRR and THR. Overall, the synergistic effects of stable char layer formation, gas-phase radical scavenging, and decreased thermal conductivity significantly decreased heat release and smoke production during combustion of RDS-wood, thereby significantly improving its flame-retardancy performance.

To conduct a more in-depth assessment of the flame retardancy of the RDS-wood, limiting oxygen index (LOI) and vertical burning tests were carried out (Fig. 7). Pristine wood was highly flammable, with an LOI value of only 21.6 % (Fig. 7a). D-wood, on the other hand, had an LOI value of 25.1 % and underwent a prolonged combustion process (Fig. 7b). The small improvement in LOI of D-wood was attributed to the densification process that eliminated the air-filled voids in the wood fiber lumens and vessels to form a tightly packed laminal structure (Fig. 3) and impeded oxygen infiltration into the material [29].

Notably, RD-wood and RDS-wood both exhibited remarkable resistance to ignition in ambient. Upon exposure to a heat source, they rapidly formed a carbon layer and self-extinguished once removed from the heat source (Fig. 7c–d). The LOI value reached an impressive value of 45.1 % for RD-wood. This significant improvement validated the effectiveness of PEI/APP impregnation in enhancing flame retardancy. After the subsequent TEOS/PDMS dip-coating, RDS-wood retained an LOI value of 41.2 %, indicating that PEI/APP largely remained within the RDS-wood matrix, as summarized in Table S3. Additionally, the silica network formed through the hydrolysis and condensation of TEOS decreased the heat transfer rate, effectively prevented the wood from reaching its ignition temperature [30,31]. Meanwhile, the adhesive-free self-curing superhydrophobic layer formed a multifunctional protective barrier that played a crucial role in mitigating the migration loss of flame retardants. In comparison, RD-wood without superhydrophobic treatment became flammable – particularly at the edges – due to the leaching of water-soluble PEI and APP after immersing in water for 48 h as evidenced by a weight loss of over 10 % (Fig. 7e) and the decrease in LOI to 33.5 %. In contrast, RDS-wood retained remarkable fire resistance with a weight loss of less than 2 % (Fig. 7f) and a great LOI at 40.5 % after water soaking (Fig. 7g). The LOI value of PEI/APP-impregnated wood without hot-pressing (R-wood) was similar to that of D-wood, exhibiting over 15 % weight loss after 48 h water soaking. Through the synergistic integration of hot-pressing and adhesive-free self-curing superhydrophobic dip-coating, the overall flame retardancy of RDS-wood is substantially maintained, ensuring efficacy even in water-exposed environments.

RDS-wood outperformed similar products reported in literature as well as a commercial class A fire-resistant fiberboard in terms of flame retardancy and hydrophobicity. Comparative analysis of RDS-wood with literature studies and a commercial class A fire-resistant fiberboard (A-MDF, ASTM E84-22) were carried out as listed in Table 1 and shown in Fig. 8. In terms of flame retardancy, RDS-wood exhibited a remarkable THR reduction of 65.6 % and an LOI of 41.2 %, significantly better than many flame-retardant woods such as SH FR-wood [15] and

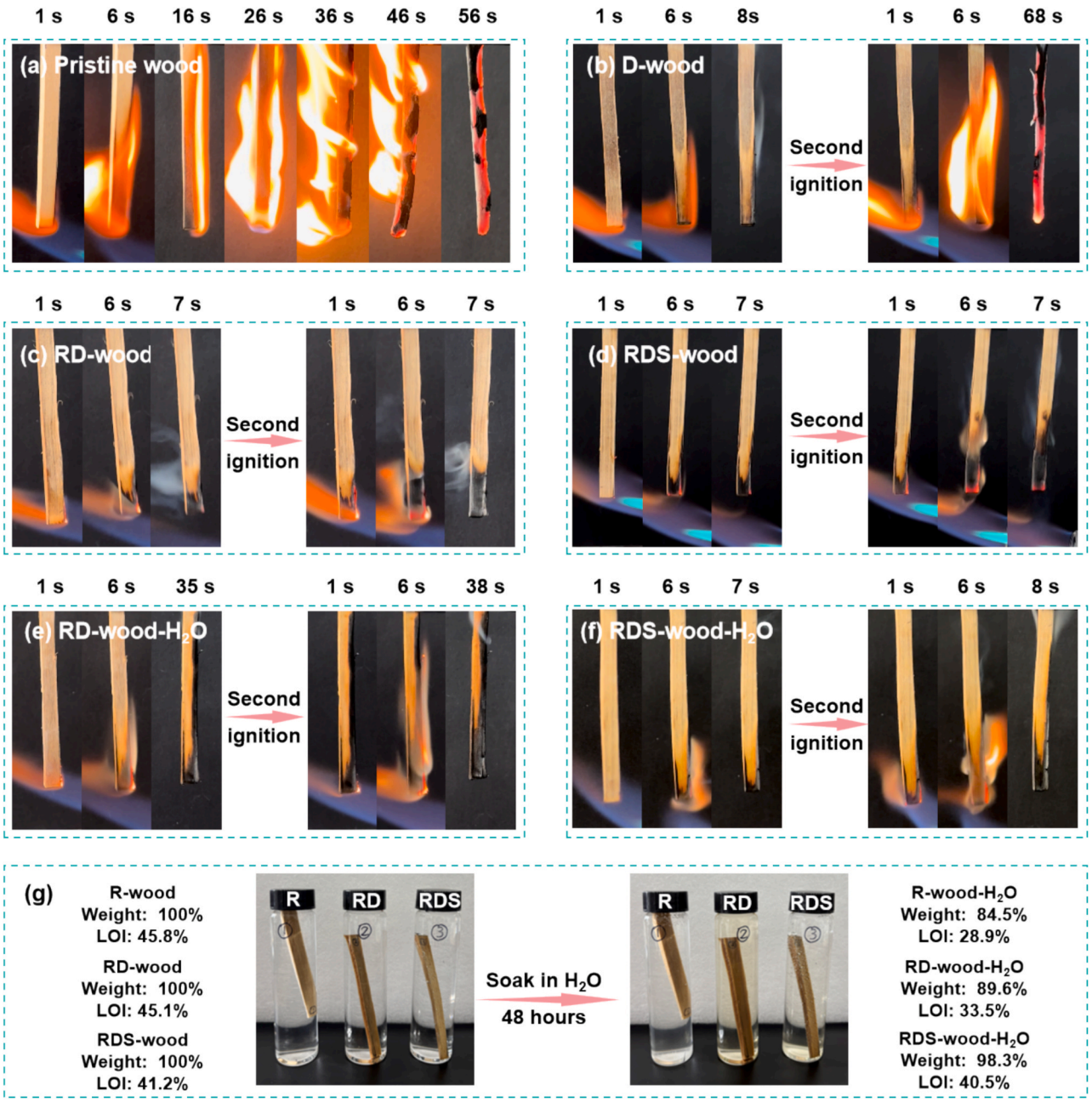

Fig. 7. Burning test images and water-soaking photographs of wood samples. (a) pristine wood. (b) D-wood. (c) RD-wood. (d) RDS-wood. (e) RD-wood soaked in water for 48 h. (f) RDS-wood soaked in water for 48 h. (g) Photographs of R-wood, RD-wood, and RDS-wood after water soaking.

PM-Fe3+/OA/wood [32]. In terms of hydrophobicity, RDS-wood has a WCA of 161.2° and SA of 3.9° also better than other superhydrophobic wood products such as HTEP/PFOES wood [17] and Mg-Al LDH-coated wood [33]. Furthermore, RDS-wood had a tensile strength of 439 MPa, substantially greater than those materials considered having great mechanical strength such as SS-TMESB bamboo [34]. Moreover, RDS-wood also exhibited better performance in flame retardancy after water soaking, in addition to greater mechanical strength and hydrophobicity when compared with the commercial class A fire-resistant fiberboard (A-MDF), as clearly demonstrated in the pie chart and radar chart in Fig. 8d. This opens greater and new markets for the present RDS-wood for broad structural applications in buildings, construction, automobiles, furniture manufacturing, interior decorations, etc.

Conclusions

This research demonstrated a dual-modification strategy that combines mechanical hot-pressing with chemical adhesive-free self-curing superhydrophobic dip-coating to mitigate the flame retardancy leaching/losses of nitrogen-phosphorus impregnated wood. By engineering a low-surface-energy hierarchical nanostructure and integrating nitrogen-phosphorus synergistic flame-retardant chemistry, the resulting wood surface exhibited superhydrophobicity and self-cleaning properties – with a water contact angle of 161.2° and a sliding rolling off angle of 3.9° – along with a substantially improved fire retardancy, e.g., a 77.7 % decrease in peak heat release rate and a 63.6 % decrease in total heat release. This strategy effectively prevented flame retardant leaching and ensured sustained long-term fire-retardant efficacy under high-humidity/wet conditions. Furthermore, hydrogen and covalent cross-linking between flame retardants and wood constituents through

Table 1
Comparison of the properties of RDS-wood with established literature techniques.

Wood	Flame retardancy: THR Reduction LOI	Hydrophobicity	Tensile strength (MPa)	Ref.
RDS-wood(PEI/APP/PDMS/TEOS)	63.6 %41.2 %	WCA: 161.2°SA: 3.9°	439	This work
SH FR-wood(ETA-APP/PER/PDMS/M−SiO_2)	34.9 %31.0 %	WCA: 154.4°SA: 3.8°	N/A	[15]
PM-Fe3+/OA/wood (MA/PA/Fe^{3+}/OA)	52.4 %38.6 %	WCA: 154.9	N/A	[32]
Mg − Al LDH-coated wood(Mg − Al LDH/TDFS)	40.0 %39.1 %	WCA: 152.0°SA: 8.6°	N/A	[33]
SS-TMESB bamboo (sodium silicate/TEOS/TMES)	21.0 %36.0 %	WCA: 147.0°	125	[34]
SH-wood(PDMS/PE)	33.8 %28.2 %	WCA: 157°SA: 2.3°	N/A	[35]
Lig-wood(*p*-TsOH pretreatment and in-situ lignin regeneration)	N/A	WCA: 148°SA: 20°	N/A	[36]
MP-3(PA/Urea/MUF)	23.4 %39.1 %	N/A	N/A	[37]
HT/EP/PFOES wood (HT/EP/PFOES)	34.5 %27.4 %	WCA: 152.6°SA: 5.4°	N/A	[17]
SPS/B-wood(SPS/H_3BO_3)	24.5 %40.3 %	N/A	N/A	[38]
WSL10(SKL/WAPMSS/Al$(OH)_3$)/H_3PO_4)	N/A27.4 %	WCA: 158°	N/A	[25]

*N/A = not available.

densification significantly enhanced wood mechanical strength with a tensile strength of 439 MPa and fracture toughness of 8.7 MJ/m3. This multifunctional wood has significant potential for applications in buildings, constructions, transportation, and other industries with stringent requirements for fire resistance, safety, weatherability, and mechanical strength.

Materials and methods

Materials

Wood veneer of Amur Linden (*Tilia amurensis Rupr.*) with dimensions of 150 mm × 900 mm × 5 mm was obtained by cutting a tree trunk along the direction of tree growth. Additionally, the knots were removed prior to any treatment. Class A Fire-Rated (ASTM E84) Medium Density Fiberboard (A-MDF) was supplied by Foshan Buylong Wood Industry Co., Ltd. Polydimethylsiloxane (PDMS, Sylgard 184) was obtained from Dow Corning Corporation. Benzyltrimethylammonium chloride (BMCl), ethanolamine (EA), polyethyleneimine (PEI, MW = 1800), ammonium polyphosphate (APP, n > 1500), tetraethyl orthosilicate (TEOS) and other chemicals were supplied by Shanghai Aladdin Biochemical Technology Co., Ltd. (China) and were used without further purification.

Fabrication of flame-retardant, tough wood, and superhydrophobic/self-cleaning wood

A wood veneer board was cut into pieces with dimensions of 100 mm (axial) × 100 mm (radial) × 5 mm (tangential) and stored in plastic bags at room temperature prior to treatment. Deep eutectic solvent BMCl/EA was first heated in an oil bath to 100 °C with a molar ratio of 1: 6. Then the prepared wood veneer samples were put into the solvent with a liquid/mass ratio of 10 (mL/g) and delignified for 4 h. At the end of the delignification, the wood veneer was removed from the solvent and washed several times with deionized water to remove residual chemicals and dissolved compounds. The wood chemical compositions along with delignification wood solid yield were listed in Table S1. Solvent BMCl/EA exhibited outstanding delignification selectivity with lignin removal of 44.3 % and glucan and xylan losses of 9.1 % and 21.1 %, respectively.

To prepare the flame-retardant solution, 11.25 g of polyethyleneimine (PEI) was first dissolved in 100 mL of deionized water at room temperature. 16.90 g of ammonium polyphosphate (APP) was subsequently added. The mixture was then stirred at 40 °C for 3 h and resulted in a transparent and stable PEI/APP solution. To prepare superhydrophobic solution, 100 mL of ethanol, 8.0 mL of tetraethyl orthosilicate (TEOS), and 4.0 g of polydimethylsiloxane (PDMS) were thoroughly mixed in a beaker using a magnetic stirrer. Aqueous ammonia was then added drop-wise to the suspension while continuously stirring at 25 °C to adjust the pH to approximately 11.

The delignified wood was initially immersed in the flame-retardant solution under ambient pressure for 12 h, followed by hot-pressing for densification at 100 °C and 5 MPa for 6 h to immobilize the flame retardant. The samples were then dip-coated with adhesive-free superhydrophobic TEOS/PDMS solution to fabricate the flame-retardant (R), mechanically strong densified (D), and superhydrophobic (S) wood composite, denoted as RDS-wood. The combined loading of the two flame retardants (APP + PEI) was 25.0 ± 3.0 wt% while the combined loading of the hydrophobic agents (TEOS + PDMS) was 2.8 ± 0.5 wt%, as the mass of the RDS-wood composite, determining the by the weight gains of the wood samples. The densified delignified wood without flame-retardant impregnation and superhydrophobic dip-coating was marked as D-wood. The delignified wood impregnated with flame-retardant without densification was marked as R-wood. The delignified wood treated with flame-retardant impregnation and densification was denoted as RD-wood. The densified delignified wood subjected to superhydrophobic dip-coating without flame-retardant impregnation was marked as DS-wood.

Wood characterizations

Attenuated total reflection-Fourier transform infrared spectroscopy (ATR-FTIR, Nicolet iS10, Thermo Scientific, USA) spectra were collected between 4000 and 650 cm^{-1} wavenumbers with 4 cm^{-1} resolution and an average of 32 scans. The wood surface chemical states of the elements were investigated by X-ray photoelectron spectroscopy (XPS, ESCA-LAB 250 X_i, Thermo Fisher Scientific, USA) using Al K_α radiation. Morphologies of surface, cross-sectional, and axial sections of the wood samples were characterized using a Scanning Electron Microscope (SEM, Nova Nano SEM 450, Frequency Electronics Inc., USA) with an accelerating voltage of 10 kV.

Mechanical properties of wood samples were tested by a SANS Model E40 electronic universal testing machine (Metus Industrial Systems Co., LTD, USA) equipped with a 30 kN load cell at a cross-head speed of 5 mm/min according to the ASTM standard D638-10. The wood specimens were cut into dumbbell-shape with a special die (R32022015, Wuhan Qien Science and Technology Development Co. LTD, China). The thermal stability of wood was analyzed using a thermogravimetric analyzer (TGA, STA 449C3/G, NETZSCH Scientific Instruments Trading Ltd., Germany) at a heating rate of 10 °C/min under a N_2 atmosphere, with the temperature ranging from 30 °C to 700 °C.

Flame retardancy of wood specimens (100 mm × 100 mm) was evaluated using a cone calorimeter (VOUCH-6810, Suzhou Yangyi Volki Testing Technology Co., LTD, China) according to ISO 5660–1: 2002 under 50 kW/m^2 external heat fluxes in an air atmosphere. Heat release rate (HRR), total heat release (THR), smoke production rate (SPR) and total smoke production (TSP) were measured. The limiting oxygen index (LOI) of wood with a sample dimension of 80 mm × 6.5 mm was measured according to the ASTM oxygen index method D2863 by a

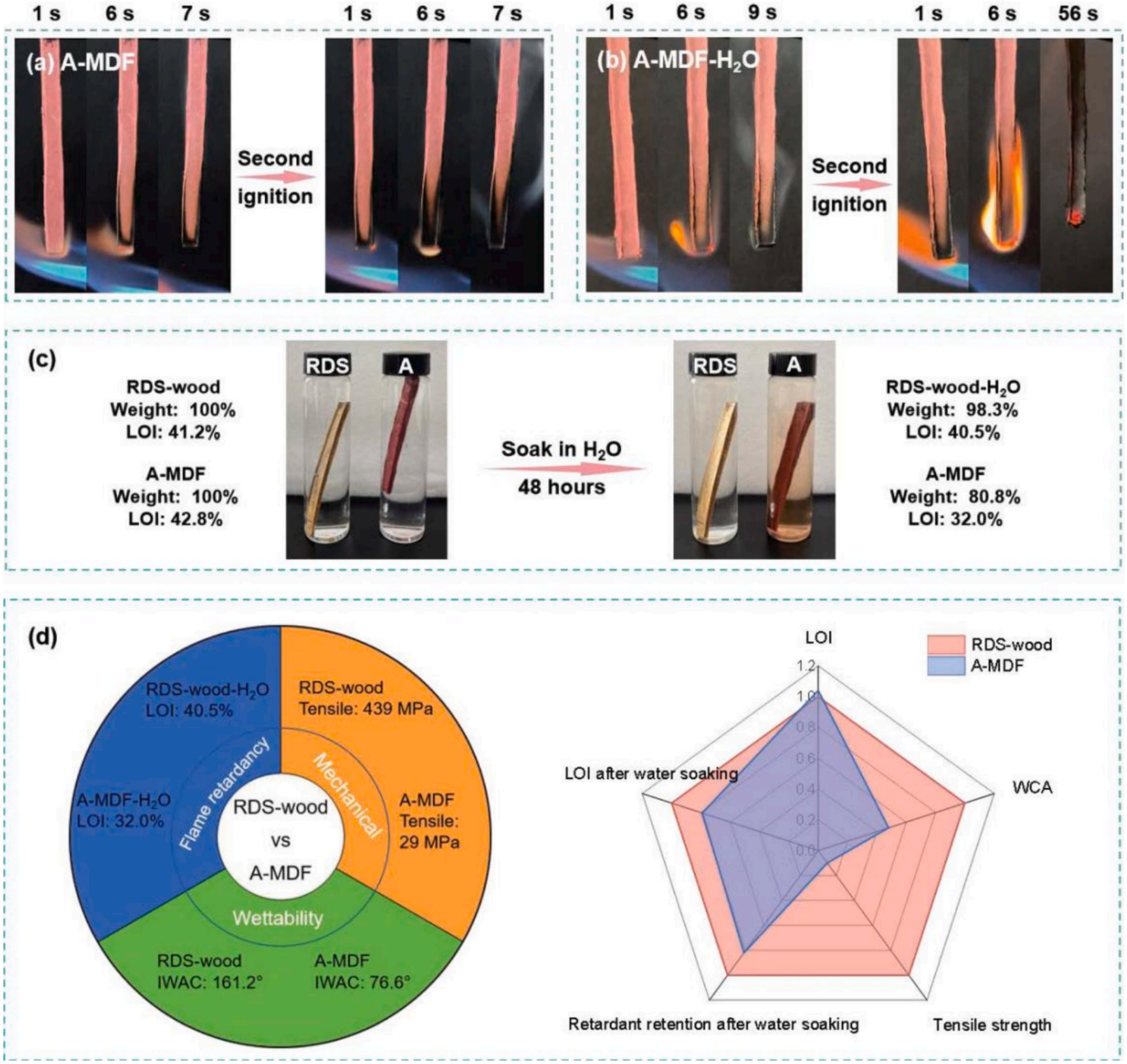

Fig. 8. Images of burning, water-soaking tests, and comparative analysis of A-MDF and RDS-wood. (a) A-MDF. (b) A-MDF soaked in water for 48 h. (c) Photographs of RDS-wood and A-MDF after water soaking. (d) Comparative analysis of RDS-wood and A-MDF.

limiting oxygen index instrument (ZR-01, Qingdao Shanfang Instrument Co., ltd., China). Duplicate runs of each test were carried out and the averages were reported.

Water contact angles (WCA) were measured by a versatile optical tensiometer (Theta Attension Tensiometer, Attension/Biolin Scientific, Espoo, Finland). The sliding angle for droplet roll-off on wood samples was measured using an adjustable angle tilting stage (MOKIN, MK-65, Boston-Shenzhen Trading Co., Ltd., China). Mechanical and chemical stabilities of superhydrophobic layer were conducted with sandpaper friction and acid-alkali-salt corrosion. For the sandpaper abrasion test, the surface of the RDS-wood was placed face-down on 1000 Cw sandpaper under a pressure applied by a 100 g weight. The RDS-wood was moved 10 cm across the sandpaper per cycle, and its contact angle was measured after 20 to 80 friction cycles, respectively. In the acid-alkali-salt corrosion test, the RDS-wood was immersed in HCl solution (pH = 2), NaOH solution (pH = 12), and NaCl solution (3.5 wt%) for 24 h. During this period, samples were periodically retrieved from each solution group, dried in an oven at 105 °C for 3 h, and subjected to measurements of WCA tests. Each test was performed in duplicates, and the reported results were the averages.

CRediT authorship contribution statement

Feng Gu: Writing – original draft, Methodology, Investigation, Formal analysis, Data curation, Conceptualization. **Xianhao He:** Writing – original draft, Methodology, Investigation, Formal analysis, Data curation, Conceptualization. **Youhang Wei:** Investigation, Formal analysis. **Xiuxue Niu:** Investigation, Formal analysis. **Zhaosheng Cai:** Writing – review & editing, Supervision. **Bo Jiang:** Writing – review & editing, Supervision. **J.Y. Zhu:** Writing – review & editing, Supervision,

Conceptualization. **Wangxia Wang:** Writing – review & editing, Supervision, Conceptualization.

Declaration of competing interest

The authors declare that they have no known competing financial interests or personal relationships that could have appeared to influence the work reported in this paper.

Acknowledgments

We acknowledge the financial support from National Natural Science Foundation of China (Nos. 21908188, 22008206), Natural Science Foundation of Jiangsu Province (Nos. BK20181051 & BK20181052). The findings and conclusions in this publication are those of authors and should not be construed to represent any official USDA or U.S. Government determination or policy.

Appendix A. Supplementary data

Supplementary data to this article can be found online at https://doi.org/10.1016/j.mattod.2025.08.034.

Data availability

Data will be made available on request.

References

[1] S. Xiao, et al., Lightweight, strong, moldable wood via cell wall engineering as a sustainable structural material, Science 374 (2021) 465–471, https://doi.org/10.1126/science.abg9556.
[2] Y. Ding, et al., Emerging engineered wood for building applications, Chem. Rev. 123 (2023) 1843–1888, https://doi.org/10.1021/acs.chemrev.2c00450.
[3] Future Resources Institute. Overview of Wildfires in the United States. 9 Apr. 2025.
[4] S.T. Lazar, T.J. Kolibaba, J.C. Grunlan, Flame-retardant surface treatments, Nat. Rev. Mater. 5 (4) (2020) 259–275, https://doi.org/10.1038/s41578-019-0164-6.
[5] M. Venier, A. Salamova, R.A. Hites, Halogenated flame retardants in the Great Lakes environment, Acc. Chem. Res. 48 (7) (2015) 1853–1861, https://doi.org/10.1021/acs.accounts.5b00180.
[6] P. Wu, et al., Flame retardancy and smoke suppression properties of bio-based chitosan polyelectrolyte flame retardant containing P and N in epoxy resin, Int. J. Biol. Macromol. 279 (2024) 135001, https://doi.org/10.1016/j.ijbiomac.2024.135001.
[7] H. Yue, et al., Flame-retardant and form-stable delignified wood-based phase change composites with superior energy storage density and reversible thermochromic properties for visual thermoregulation, ACS Sustainable Chem. Eng. 11 (2023) 3932–3943, https://doi.org/10.1021/acssuschemeng.2c07635.
[8] Y. Liu, et al., Nb_2CT_x MXene/starch hybrid aerogels supported flame-retardant phase change composites with superior solar-thermal conversion efficiency and outstanding electromagnetic interference shielding, Compo. Part A 193 (2025) 108854, https://doi.org/10.1016/j.compositesa.2025.108854.
[9] Z. Huang, et al., High-efficiency ammonium polyphosphate intumescent encapsulated polypropylene flame retardant, J. Appl. Polym. Sci. 138 (20) (2021) 50413, https://doi.org/10.1002/app.50413.
[10] F. Xu, H. Zhang, J. Wu, Synergistic catalytic flame retardant effect of zirconium phosphate on the poplar plywood, Constr. Build. Mater. 290 (2021) 123208, https://doi.org/10.1016/j.conbuildmat.2021.123208.
[11] D. Lin, et al., One-pot fabrication of superhydrophobic and flame-retardant coatings on cotton fabrics via sol-gel reaction, J. Colloid Interf. Sci. 533 (2019) 198–206, https://doi.org/10.1016/j.jcis.2018.08.060.
[12] B. Östman, et al., Durability of fire retardant treated wood products at humid and exterior conditions review of literature, Fire Mater. 25 (3) (2001) 95–104, https://doi.org/10.1002/fam.758.
[13] X. Tian, T. Verho, R.H.A. Ras, Moving superhydrophobic surfaces toward real-world applications, Science 352 (2016) 142–143, https://doi.org/10.1126/science.aaf2073.
[14] H.J. Butt, et al., Characterization of super liquid-repellent surfaces, Curr. Opin. Colloid in. 19 (2014) 343–354, https://doi.org/10.1016/j.cocis.2014.04.009.
[15] R. Sun, et al., Formulation of environmentally robust flame-retardant and superhydrophobic coatings for wood materials, Constr. Build. Mater. 392 (2023) 131873, https://doi.org/10.1016/j.conbuildmat.2023.131873.
[16] L. Xu, et al., Highly flexible and superhydrophobic MOF nanosheet membrane for ultrafast alcohol-water separation, Science 378 (2022) 308–313, https://doi.org/10.1126/science.abo5680.
[17] S. Jia, et al., A new insight into the design of robust superhydrophobic and fire retardant wood: breaking the conflicting requirement on adhesives, Chem. Eng. J. 475 (2023) 146240, https://doi.org/10.1016/j.cej.2023.146240.
[18] L. Guo, J. Hyeon-Lee, G. Beaucage, Structural analysis of poly(dimethylsiloxane) modified silica xerogels, J. Non-Crystalline Solids 243 (1) (1999) 61–69, https://doi.org/10.1016/S0022-3093(98)00819-9.
[19] D. Lin, et al., One-pot fabrication of superhydrophobic and flame-retardant coatings on cotton fabrics via sol-gel reaction, J. Colloid Interf. Sci. 533 (2019) 198–206, https://doi.org/10.1016/j.jcis.2018.08.060.
[20] H. Shen, et al., Multifunctional wood composites featuring synergistic flame retardant, smoke suppression, and superhydrophobic functionalities, Ind. Crop Prod. 228 (2025) 120852, https://doi.org/10.1016/j.indcrop.2025.120852.
[21] F. Wang, et al., A superhydrophobic coating to create multi-functional materials with mechanical/chemical/physical robustness, Chem. Eng. J. 381 (2020) 122539, https://doi.org/10.1016/j.cej.2019.122539.
[22] C. Ruan, et al., A superhydrophobic sponge with excellent absorbency and flame retardancy, Angew. Chem. Int. Ed. 53 (2014) 5556–5560, https://doi.org/10.1002/anie.201400775.
[23] R.N. Wenzel, Resistance of solid surfaces to wetting by water, Ind. Eng. Chem. 28 (8) (1936) 988–994.
[24] A.B.D. Cassie, S. Baxter, Wettability of porous surfaces, Trans. Faraday Soc. 40 (1944) 546–551.
[25] B. Kassaun, P. Fatehi, Solvent-free lignin-silsesquioxane wood coating formulation with superhydrophobic and flame-retardant functionalities, Chem. Eng. J. 493 (2024) 152582, https://doi.org/10.1016/j.cej.2024.152582.
[26] Y. Fang, et al., Durable flame retardant and anti-dripping of pet fabric using bio-based covalent crosslinking intumescent system of chitosan and phytic acid, Prog. Org. Coat. 183 (2023) 107785, https://doi.org/10.1016/j.porgcoat.2023.107785.
[27] M. Zhi, et al., A comprehensive review of reactive flame-retardant epoxy resin: Fundamentals, recent developments, and perspectives, Polym. Degrad. Stab. 201 (2022) 109976, https://doi.org/10.1016/j.polymdegradstab.2022.109976.
[28] C. Yan, et al., Imparting hydrophobicity and flame retardancy to wood using functionalized carbon nanotubes compounded with ammonium polyphosphate, Constr. Build. Mater. 472 (2025) 140886, https://doi.org/10.1016/j.conbuildmat.2025.140886.
[29] W. Gan, et al., Dense, self-formed char layer enables a fire-retardant wood structural material, Adv. Funct. Mater. 29 (2019) 1807444, https://doi.org/10.1002/adfm.201807444.
[30] L. Liu, et al., Finishing of cotton fabrics by multi-layered coatings to improve their flame retardancy and water repellency, Cellul. 25 (8) (2018) 4791–4803, https://doi.org/10.1007/s10570-018-1866-4.
[31] C. Su, et al., Multifunctional design integrating the flame-retardant and antifouling functionality into superhydrophobic cotton fabric, Prog. Org. Coat. 185 (2023) 107871, https://doi.org/10.1016/j.porgcoat.2023.107871.
[32] L. Ma, et al., Preparation of multifunctional flame-retardant and superhydrophobic composite wood by iron ions doped phytic acid-based nanosheets, Constr. Build. Mater. 422 (2024) 135854, https://doi.org/10.1016/j.conbuildmat.2024.135854.
[33] B. Guo, et al., Efficient flame-retardant and smoke-suppression properties of Mg–Al-layered double-hydroxide nanostructures on wood substrate, ACS Appl. Mater. Interfaces 9 (27) (2017) 23039–23047, https://doi.org/10.1021/acsami.7b06803.
[34] L. He, et al., Synergistic enhancement of flame retardancy, mechanical properties, dimensional stability, and mold resistance in bamboo via silica mineralization and hydrophobic treatment, Chem. Eng. J. 510 (2025) 161505, https://doi.org/10.1016/j.cej.2025.161505.
[35] X. Yao, et al., Preparation of wood-based surface coatings with dual functions of flame retardancy and superhydrophobicity by sand-in method, Prog. Org. Coat. 204 (2025) 109244, https://doi.org/10.1016/j.porgcoat.2025.109244.
[36] X. Shi, et al., Native lignin migration and clustering in wood: Superhydrophobic, antimold, and tribonegative layers for rain-driven electrification, Adv. Funct. Mater. (2025) 2504381, https://doi.org/10.1002/adfm.202504381.
[37] F. Song, et al., Sustainable, high-performance, flame-retardant waterborne wood coatings via phytic acid based green curing agent for melamine-urea-formaldehyde resin, Prog. Org. Coat. 162 (2022) 106597, https://doi.org/10.1016/j.porgcoat.2021.106597.
[38] K. Wang, et al., A facile preparation of environmentally-benign and flame-retardant coating on wood by comprising polysilicate and boric acid, Cellul. 28 (18) (2021) 11551–11566, https://doi.org/10.1007/s10570-021-04238-2.